

A double stellar generation in the Globular Cluster NGC 6656 (M 22).[★]

Two stellar groups with different iron and *s*-process element abundance.

A. F. Marino^{1,2}, A. P. Milone¹, G. Piotto¹, S. Villanova³, L. R. Bedin⁴, A. Bellini^{1,4}, and A. Renzini⁵

¹ Dipartimento di Astronomia, Università di Padova, Vicolo dell'Osservatorio 3, Padova, I-35122, Italy, EU
e-mail: anna.marino, antonino.milone, giampaolo.piotto, andrea.bellini@unipd.it

² P. Universidad Católica de Chile, Departamento de Astronomía y Astrofísica, Casilla 306, Santiago 22, Chile
e-mail: fmarino@astro.puc.cl

³ Departamento de Astronomia, Universidad de Concepcion, Casilla 160-C, Concepcion, Chile
e-mail: svillanova@astro-udec.cl

⁴ Space Telescope Science Institute, 3700 San Martin Drive, Baltimore, MD 21218, USA
e-mail: bedin, bellini@stsci.edu

⁵ Osservatorio Astronomico di Padova, Vicolo dell'Osservatorio 5, 35122 Padova, Italy
e-mail: alvio.renzini@oapd.inaf.it

Received XXXX xx, xxxx; accepted XXXX xx, xxxx

Abstract. *Aims.* In this paper we present the chemical abundance analysis from high resolution UVES spectra of seventeen bright giant stars of the Globular Cluster (GC) M 22.

Results. We obtained an average iron abundance of $[\text{Fe}/\text{H}] = -1.76 \pm 0.02$ (internal errors only) and an α enhancement of 0.36 ± 0.04 (internal errors only). Na and O, and Al and O follow the well known anti-correlation found in many other GCs. We identified two groups of stars with significantly different abundances of the *s*-process elements Y, Zr and Ba. The relative numbers of the two group members are very similar to the ratio of the stars in the two SGBs of M 22 recently found by Piotto (2009). Y and Ba abundances do not correlate with Na, O and Al. The *s*-element rich stars are also richer in iron and have higher Ca abundances.

The results from high resolution spectra have been further confirmed by lower resolution GIRAFFE spectra of fourteen additional M 22 stars. GIRAFFE spectra show also that the Eu – a pure *r*-process element – abundance is not related to the iron content. We discuss the chemical abundance pattern of M 22 stars in the context of the multiple stellar populations in GC scenario.

Key words. Spectroscopy — globular clusters: individual: NGC 6656

1. Introduction

Globular Clusters (GC) are generally chemically homogeneous in their Fe-peak elements, while they show star-to-star abundance variations in light elements like C, N, O, Na, Mg, Al among others. In some cases, these chemical inhomogeneities result in well defined anticorrelations. For example, all GCs for which Na and O abundances have been measured, show a well defined NaO anti-correlation (see Carretta et al. 2006, 2008 for an update), often associated with an anti-correlation between Mg and Al contents. The origin of these variations has not yet been well understood, since both a primordial and an evolution-

ary explanation, or a combination of both have been proposed (see Gratton et al. 2004 for a recent review).

Interestingly enough, abundance anomalies have been found also among stars in the lower part of the red giant branch (RGB) or even in the main sequence (MS). E.g., Cannon et al. (1998) found a CN bi-modality in MS and sub giant branch (SGB) stars in 47 Tuc, and the NaO anti-correlation was observed at the level of MS Turn Off (TO) and SGB in M 13 (Cohen & Melendez 2005), NGC 6397 and NGC 6752 (Carretta et al. 2005; Gratton et al. 2001), NGC 6838 (Ramírez & Cohen 2002). By themselves, these results suggest the possibility of a primordial origin for the abundance inhomogeneities.

More recent results, made possible by a significant improvement of the photometric precision on *HST* images, indicating the presence of multimodal sequences in the color-

Send offprint requests to: XXX. XXX.

[★] Based on data collected at the European Southern Observatory with the VLT-UT2, Paranal, Chile.

magnitude diagrams (CMD) of some GCs (Bedin et al. 2004, Piotto et al. 2007, Milone et al. 2008, and Piotto et al. in preparation) further confirm that at least in some GCs there is more than one generation of stars formed from material chemically contaminated by previous generations.

Among the clusters with multiple stellar populations, ω Centauri is the most complex and interesting case. This object is the only one for which variations in iron-peak elements have been certainly identified (Freeman & Rodgers 1975; Norris et al. 1996; Suntzeff & Kraft 1996). The Fe multimodal distribution is at least in part responsible of the multiple RGB (Lee et al. 1999, Pancino et al. 2000) of ω Cen. Also the MS of this GC splits into three sequences as shown by Bedin et al. (2004). Among the two principal MSs, the bluest one is more metal rich than the redder one (Piotto et al. 2005). So far, the only way we have to explain the photometric and spectroscopic properties of the MS of ω Cen is to assume that the bluest MS is also strongly He-enhanced. Recently, Villanova et al. (2007) showed that also the SGB splits in at least four branches with a large age difference (larger than 1 Gyr) among the different populations.

NGC 2808 is the second (in time) cluster in which a MS split into three branches was found (Piotto et al. 2007). Also in this case, the MS multimodality was associated with different values of Helium, to the observed multimodal distribution of the stars along the NaO anti-correlation, where three groups of stars with different O (and Na) content were found by Carretta et al. (2006).

In NGC 1851 Yong & Grundahl (2008) found abundance variations in various elements by studying a sample of 8 RGB stars. Sodium and oxygen follow the NaO anti-correlation. There is also some evidence for the presence of two groups of stars with different *s*-process element content, as well as of two groups of stars with different CN-strength, that are possibly related to the two sequences photometrically identified by Milone et al. (2008) along the SGB. The split SGB of NGC 1851 can be explained as due to the presence of two stellar populations. The stars in the fainter SGB could either be part of a population about 1 Gyr older than the bright SGB one, or could indeed be slightly younger than the bright SGB ones, but strongly enriched in total C+N+O content (Cassisi et al. 2008).

Another recent evidence for a primordial origin of abundance variations related to the presence of different populations of stars comes from Marino et al. (2008). By studying a large sample of RGB stars in the GC M 4, they found two distinct groups of stars with a different sodium content, which also display a remarkable difference in the strength of the CN-band. These two spectroscopic groups were found to populate two different regions along the RGB. They also noted that the RGB spread is present from the base of the RGB to the RGB-tip, suggesting that the spread must be related to the presence of two distinct stellar generations.

At the basis of the present investigation, there is a very recent result by our group, who identified a bimodal distribution of the stars in the SGB of the GC NGC 6656 (Piotto 2009, see Fig. 18 in the present paper).

Located at a distance from the Sun of ~ 3.2 kpc (Harris 1996), NGC 6656 (M 22) is a particularly interesting GC, be-

cause a large number of photometric and spectroscopic studies suggested a complex metallicity spread, similar to, albeit significantly smaller than, that found in ω Centauri. In particular, it has been often suggested, though never convincingly confirmed, that M 22 may have also a spread in the content of iron peak elements.

The first evidence for a spread in metallicity comes from the significant spread along the RGB (Hesser et al. 1977; Peterson & Cudworth 1994) observed both in $(B - V)$ and in Strömgren colors. However, it is still uncertain whether this spread can be attributed to a metallicity spread or to reddening variations. Due to its location on the sky, close to the Galactic plane and toward the Galactic Bulge [$(b, \ell) \simeq (10^\circ, 7^\circ)$], M 22 is affected by high and spatially varying interstellar absorption, with a reddening in the interval $0.3 < E(B - V) < 0.5$. This differential reddening creates a degeneracy in measuring metallicity when the atmospheric parameters of the stars are derived from their color. Spectroscopic studies are divided between those which conclude that no significant metallicity variations is present in M 22 (Cohen 1981, based on 3 stars; Gratton 1982, 4 stars) and studies claiming a spread in iron, with $-1.4 < [\text{Fe}/\text{H}] < -1.9$ (Pilachowsky et al. 1984, 6 stars; Lehnert et al. 1991, 4 stars).

Particularly interesting are the findings on CN-band strengths. Norris & Freeman (1983) showed that CN variations in M 22 were correlated with Ca, H and K line variations, similar to those in ω Cen. By studying a sample of 4 stars, Lehnert et al. (1991) found Ca and Fe variations that also correlated with variations in CH and CN band strength. However, Brown & Wallerstein (1992) found no Ca abundance differences between CN-strong and CN-weak stars, though they observed differences in $[\text{Fe}/\text{H}]$ correlating with the CN-strength. More recently, Kayser et al. (2008) found some indications of a CN-CH anti-correlation in SGB stars, maybe diluted by large uncertainties introduced by differential reddening.

In the present study we analyze high resolution UVES spectra for a sample of seventeen RGB stars in M 22 in order to study the chemical abundances and possible relations with the recently found SGB split. In order to increase the statistical significance and reinforce our findings, we also added the results from a sample of fourteen RGB stars from medium resolution, high S/N GIRAFFE spectra. In Section 2 we provide an overview of the observations and of the data analysis, and in Section 3 we describe the procedure used to derive the chemical abundances. Our results on the chemical composition of M 22 are presented in Section 4, and a discussion on them is provided in Section 5. In Section 6 we look for possible connections between our spectroscopic results and the two stellar populations photometrically observed by Piotto (2009). A comparison between the results of this paper and those of Marino et al. (2008) on the GC M 4 is provided in Section 7. In Section 8 we present a brief discussion on the results obtained from GIRAFFE spectra. Section 9 summarizes the most relevant properties of the two stellar populations of M 22.

2. Observations and membership analysis

Our data set consists of spectra of seventeen RGB stars retrieved from the ESO archive. The observations were ob-

Table 1. Right Ascension, Declination, Heliocentric radial velocities, and magnitudes for the analyzed stars.

ID	RA [degree]	DEC [degree]	RV _H [km s ⁻¹]	<i>B</i>	<i>V</i>	<i>I</i>
71	279.032271	-23.848980	-136.74	13.7458	12.3171	10.6334
88	279.150166	-23.837640	-151.21	13.9042	12.5003	10.9469
51	279.107744	-23.932690	-166.65	13.6157	12.0413	10.3165
61	279.087911	-23.945560	-145.81	13.6269	12.2122	10.5598
224	279.056427	-23.915140	-147.87	14.6701	13.4704	12.0023
221	279.137364	-23.916380	-156.45	14.6746	13.4606	11.9562
200043	279.133958	-23.934417	-152.90	13.4254	11.9082	10.1801
200025	279.042375	-23.906056	-153.22	13.2488	11.5217	9.6761
200068	279.133875	-23.858667	-139.10	13.7589	12.2961	10.6084
200031	279.113999	-23.857222	-142.08	13.1504	11.6354	9.9282
200076	279.085417	-23.940111	-158.38	13.7089	12.3647	10.7539
200101	279.159833	-23.900361	-131.00	14.0444	12.6726	11.0746
200080	279.136750	-23.852972	-147.42	13.7257	12.4310	10.8985
200104	279.083958	-23.931611	-133.25	13.9028	12.6644	11.1595
200083	279.127417	-23.880083	-129.00	–	12.4350	10.8732
200006	279.072917	-23.907249	-148.16	12.8797	11.0304	9.0975
200005	279.171042	-23.971999	-149.84	12.7874	10.9295	8.9453

tained using UVES (Dekker et al. 2000) and FLAMES@UVES (Pasquini et al. 2002). The spectra cover the wavelength range 4800-6800 Å, have a resolution $R \approx 45000$, and have a typical $S/N \sim 100 - 120$.

Data were reduced using UVES pipelines (Ballester et al. 2000), including bias subtraction, flat-field correction, wavelength calibration, sky subtraction, and spectral rectification. The membership of the analyzed stars was established from the radial velocities obtained using the IRAF@FXCOR task, which cross-correlates the object spectrum with a template. As template, we used a synthetic spectrum obtained through the spectral synthesis code SPECTRUM (see <http://www.phys.appstate.edu/spectrum/spectrum.html> for more details), using a Kurucz model atmosphere with roughly the mean atmospheric parameters of our stars $T_{\text{eff}} = 4500$ K, $\log(g) = 1.3$, $v_t = 1.6$ km/s, $[\text{Fe}/\text{H}] = -1.70$. At the end, each radial velocity was corrected to the heliocentric system. We obtained a mean radial velocity of -146 ± 2 km/s from all the selected spectra, which agrees well with the values in the literature (Peterson & Cudworth 1994). Within 2σ , where σ is our measured velocity dispersion of 10 km/s, all our stars are members. The list of the analyzed stars, their coordinates, radial velocities, and magnitudes, are reported in Table 1. Figure 1 shows the location of the target stars in the CMD of M 22.

We also analysed a sample of stars observed with GIRAFFE HR09, HR13, and HR15 set-ups at a resolution of $R \sim 20000-25000$. These spectra were reduced by using the pipeline developed by Geneva observatory (Blecha et al. 2000). More details on these data and their analysis are provided in Section 8.

3. Abundance analysis

Abundances for all elements, with the exception of oxygen, were measured from an equivalent width analysis by using the Local Thermodynamical Equilibrium (LTE) program MOOG (freely distributed by C. Sneden, University of Texas at Austin).

The atmospheric parameters, i.e. temperature, gravity, and micro-turbulence, were determined from Fe lines by removing trends in the Excitation Potential (EP) and Equivalent Widths (EW) vs. abundance respectively, and satisfying the ionization equilibrium.

At odd with other elements, we measured O content by comparing observed spectra with synthetic ones, because of the blending of the target O line at 6300 Å with other spectral features.

More details on the line-list, atmospheric parameters and abundance measurements can be found in Marino et al. (2008). In Table 2 we report the reference chemical abundances obtained for the Sun used in this paper. The obtained stellar parameters for the M 22 analyzed stars are listed in Table 3.

Table 2. Measured solar abundances ($\log \epsilon(X) = \log(N_X/N_H) + 12$).

Element	abund.	# lines	Element	abund.	# lines
O	8.83	1	Ti _{III}	4.96	12
Na	6.31	4	V	3.89	17
Mg	7.54	3	Fe _{FeI}	7.48	145
Al	6.43	2	Fe _{FeII}	7.51	14
Si	7.61	13	Ni	6.26	47
Ca	6.39	16	Y _{YII}	2.24	8
Sc _{ScII}	3.12	12	Zr _{ZrII}	2.37	1
Ti _{TiI}	4.94	33	Ba _{BaII}	2.45	2

It is important to remark here that the method employed for the measurements of the atmospheric parameters is based on the spectra, and hence our temperatures are not color dependent. This is an important advantage in analyzing GC, as M 22, affected by high differential reddening.

In Fig. 1 we marked with red symbols the location of our seventeen UVES target stars on the *B* vs. (*B* - *I*) CMD. Photometry has been obtained with the Wide Field Imager (WFI) camera at the ESO/MPI 2.2 m telescope by Monaco

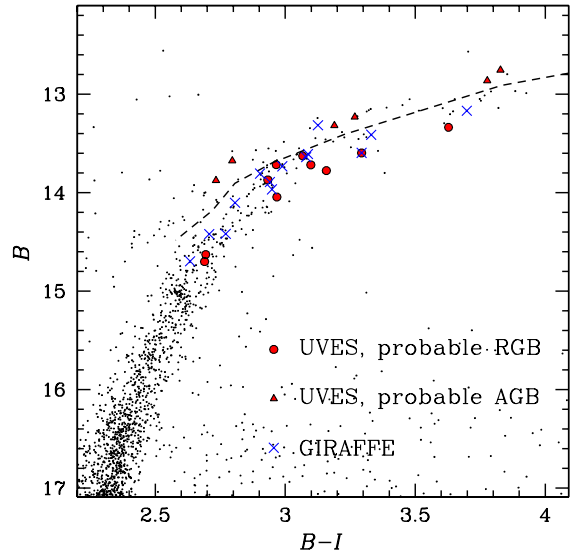
Table 3. Atmospheric parameters for the analyzed stars.

ID	T_{eff} [K]	$\log(g)$	v_t [km s $^{-1}$]	[Fe/H] [dex]
71	4460	1.15	1.44	-1.76
88	4460	1.15	1.55	-1.70
51	4260	0.90	1.60	-1.63
61	4430	1.05	1.70	-1.78
224	4700	1.70	1.45	-1.76
221	4750	1.66	1.20	-1.75
200043	4400	1.01	1.70	-1.77
200025	4100	0.67	1.80	-1.62
200068	4500	1.30	1.52	-1.84
200031	4300	0.77	1.55	-1.85
200076	4500	1.23	1.35	-1.83
200101	4500	1.35	1.55	-1.74
200080	4600	1.00	1.45	-1.81
200104	4700	1.35	1.75	-1.92
200083	4490	1.46	1.66	-1.63
200006	3990	0.20	2.08	-1.66
200005	4000	0.05	2.02	-1.94

Table 4. The average abundance for M 22 stars.

El.	Abundance [dex]	σ_{obs}	N_{stars}
[O/Fe]	0.28±0.05	0.20	17
[Na/Fe]	0.24±0.08	0.30	17
[Mg/Fe]	0.39±0.03	0.11	17
[Al/Fe]	0.34±0.08	0.31	17
[Si/Fe]	0.43±0.01	0.03	17
[Ca/Fe]	0.31±0.02	0.07	17
[Sc/Fe] _{ScII}	0.04±0.01	0.04	17
[Ti/Fe] _{TiI}	0.24±0.01	0.06	17
[Ti/Fe] _{TiII}	0.34±0.01	0.06	17
[V/Fe]	-0.09±0.02	0.10	17
[Cr/Fe]	-0.13±0.02	0.08	17
[Fe/H]	-1.76±0.02	0.10	17
[Ni/Fe]	-0.07±0.01	0.04	17
[Y/Fe] _{YII}	0.05±0.07	0.27	17
[Zr/Fe] _{ZrII}	0.36±0.06	0.23	17
[Ba/Fe] _{BaII}	0.19±0.06	0.23	17

et al. (2004) and stars with the highest photometric quality were carefully selected. Magnitudes have been corrected for sky concentration (i.e. the increasing of the background level in frames near the center due to light reflected back from the detector to the optics.) by using the best available solution (Bellini et al. 2009). Since the photometry is affected by spatially variable interstellar reddening, we have corrected the CMD for this effect (by using the method described in Sarajedini et al. 2007). To separate probable asymptotic giant branch (AGB) from RGB stars, we have drawn by hand the black dashed line of Fig. 1. Stars that, on the basis of their position in the CMD, are possible AGB stars, will be marked from here on as triangles, while RGB stars with circles.

**Fig. 1.** Distribution of the UVES target stars (red symbols) on the B vs. $(B - I)$ CMD corrected for differential reddening. The star #200083 is not plotted because the B magnitude is not available for this star. The stars observed with GIRAFFE are shown by blue crosses.

3.1. Internal errors associated to chemical abundances

The main goal of this paper is to study the intrinsic variation of chemical abundances affecting M 22 stars.

The differences in the measured chemical abundances from star-to-star are a consequence of both measurements errors and intrinsic variations in their chemical composition. In this section, our final goal is to disentangle between internal errors, due to measurements uncertainties, and real variations in the chemical content of the stars. To this aim, we will compare the observed dispersion in the chemical abundances σ_{obs} , listed in Table 4, with that produced by internal errors σ_{tot} . Since we are interested in the study of star-to-star intrinsic abundance variations, we do not treat possible external sources of errors that do not affect relative abundances.

Two sources of errors mainly contribute to σ_{tot} : the uncertainties in the EWs, and the uncertainties in the atmospheric parameters.

In order to derive the typical error in the EWs, we consider two stars (#200101 and #71) with similar atmospheric parameters and roughly the same iron abundance. In this way, any difference in the EWs in the iron spectral lines, can be attributed to measurement errors. The dispersion of the distribution of the differences between the EWs of the iron lines of the two selected stars, that is 2.3 mÅ, has been taken as our estimate of the typical error in the EWs measurement. The corresponding error in the chemical abundances has been calculated by varying the EWs of a star (#200101) at intermediate temperature, representative of our sample, by 2.3 mÅ. The variations in the obtained abundances for each chemical specie, listed in Table 5

(column 7), have been taken as our best estimate of the internal errors introduced by uncertainties in the EWs.

We used the same procedure described in Marino et al. (2008) in order to estimate the uncertainties associated to the atmospheric parameters, and the corresponding errors related to chemical abundances. From our analysis, the obtained uncertainties related to atmospheric parameters are: $\Delta T_{\text{eff}} = \pm 50$ K, $\Delta \log(g) = \pm 0.14$, and $\Delta v_t = \pm 0.13$ km/s. These internal errors in the atmospheric parameters translate into the errors in chemical abundances listed in Table 5 (columns 2, 3 and 4).

We investigated also the influence of a variation in the total metallicity ($[A/H]$) of the model atmosphere on the derived abundances. By varying the metallicity of the model by 0.10 dex, that is the iron observed dispersion, the element abundances change by the amount listed in Col. 5 of Table 5. A variation in the metallicity of the model atmosphere mainly changes the ionization equilibrium, and hence the values of $\log(g)$, since we used the ionization equilibrium between FeI and FeII to derive gravities. We calculated that by increasing $[A/H]$ by 0.10 dex, $\log(g)$ decreases by ~ 0.06 , while temperature and microturbulence do not change significantly. Since we are interested in the search for possible small star-to-star variations of iron abundances, we measured the effect in the $[Fe/H]$ abundances due to this change in gravity in a model atmosphere with increased metallicity, and verified that it does not affect the derived iron abundances by more than 0.01 dex. By increasing the total metallicity by 0.2 dex, the FeII abundances change by ~ 0.06 dex, and we have to decrease $\log(g)$ by ~ 0.12 to re-establish the ionization equilibrium between FeI and FeII. Also in this case the effect on the iron abundances is smaller than 0.01 dex.

Column 9 of Table 5 reports the quadratic sum (σ_{tot}) of the errors coming from the EWs (σ_{EW}) and from the atmospheric parameters (σ_{atm}) uncertainties. Column 8 gives the observed dispersion (σ_{obs}).

Since the oxygen abundance was calculated from the same spectral line and the spectra have similar S/N, we assume as an estimate of the error related to $[O/Fe]$, the σ_{tot} calculated in Marino et al. (2008) for M 4 red giants. This error, for M 4 stars, was calculated as the dispersion in O of the O-rich stars, i.e. the Na-poor group, assumed to be homogeneous in oxygen content.

4. The chemical composition of M 22

4.1. Iron-peak and α elements

The wide spectral range of UVES data allows us to obtain chemical abundances for fifteen chemical species. Table 4 gives the mean abundance for each element (Col. 2), the rms of the mean of the abundances σ_{obs} (Col. 3), and the number of stars (N_{stars}) used to calculate the mean (Col. 4). In Table 4, to each average abundance we associated an uncertainty which is the rms scatter (σ_{obs}) divided by $\sqrt{N_{\text{stars}} - 1}$, although some of the distributions are clearly not Gaussians. A plot of our measured abundances is shown in Fig. 2, where, for each box, the central horizontal line is the mean value for each element, and the upper and lower lines contain the 68.27% of the distribu-

tion around the mean. The points represent individual measurements.

Our results confirm M 22 to be a metal poor GC with a mean metallicity:

$$[Fe/H] = -1.76 \pm 0.02 \text{ dex}, \quad \sigma_{\text{obs}} = 0.10$$

where σ_{obs} is the rms of the 17 measurements. The iron-peak elements Ni, Cr, and V have abundances of $[Ni/Fe] = -0.07 \pm 0.01$, $[Cr/Fe] = -0.13 \pm 0.02$, and $[V/Fe] = -0.09 \pm 0.02$, respectively.

We measured the chemical abundances for five α elements: O, Mg, Si, Ca and Ti. The corresponding abundances are listed in Table 4. Here we consider only Mg, Si, Ca, and Ti. The results for oxygen will be discussed in Section 4.2. These four α elements are all overabundant with respect to solar values, with an average of:

$$[\alpha/Fe] = +0.36 \pm 0.04$$

For calcium we obtained a mean value of $[Ca/Fe] = +0.31 \pm 0.02$, similar to that found in other GCs. Interestingly enough, our stars show quite a large dispersion ($\sigma_{\text{obs}} = 0.07$, see Table 4) in the Ca abundance. This spread will be discussed more in detail in Section 5.

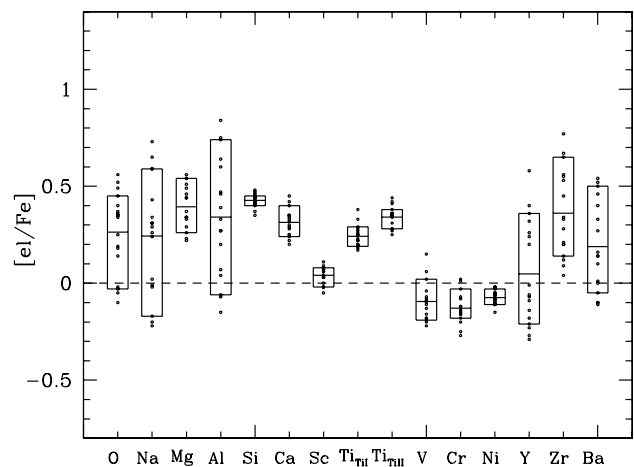


Fig. 2. Box plot for M 22 star elements abundances. The points are the individual measurements. The central horizontal line of each box is the mean of the data; the upper and lower lines contain the 68.27% of the distribution around the mean value.

4.2. NaO anti-correlation

As displayed in Fig. 3, sodium and oxygen show the typical NaO anti-correlation found in RGB stars in all GCs where Na and O have been measured so far (see Carretta et al. 2006). The $[Na/Fe]$ values range from ~ -0.25 to ~ 0.7 dex, with a dispersion $\sigma_{\text{obs}} = 0.30$, and $[O/Fe]$ abundances cover the interval from ~ -0.10 to $\sim +0.5$ dex, with a dispersion $\sigma_{\text{obs}} = 0.20$.

As it will be discussed in Section 6, Piotto (2009) have shown that the SGB of M 22 is split into two separate branches, indicating the presence of two stellar populations. In Fig. 4 we

Table 5. Sensitivity of derived UVES abundances to the atmospheric parameters and EWs. We reported the error σ_{atm} due to the uncertainties in the atmospheric parameters (ΔT_{eff} , $\Delta \log(g)$, Δv_t , and $\Delta([A/H])$) due to the error in EW measurements (σ_{EW}), the squared sum of the two (σ_{tot}), and the observed dispersion (σ_{obs}) for each element.

	ΔT_{eff} [K]	$\Delta \log(g)$	Δv_t [km s $^{-1}$]	$\Delta([A/H])$ [dex]	σ_{atm}	σ_{EW}	σ_{tot}	σ_{obs}
	+50	+0.14	+0.13	+0.10				
[O/Fe]	–	–	–	–	–	–	0.04	0.20
[Na/Fe]	–0.02	–0.01	+0.01	–0.01	0.03	0.01	0.03	0.30
[Mg/Fe]	–0.03	+0.00	+0.01	–0.01	0.03	0.02	0.04	0.11
[Al/Fe]	–0.03	–0.01	+0.02	–0.01	0.04	0.06	0.07	0.31
[Si/Fe]	–0.05	+0.01	+0.01	+0.01	0.05	0.01	0.05	0.03
[Ca/Fe]	–0.01	–0.01	–0.01	–0.01	0.02	0.01	0.02	0.07
[Sc/Fe]	+0.03	+0.00	+0.00	+0.00	0.03	0.03	0.04	0.04
[Ti/Fe] _{TII}	+0.04	–0.01	+0.00	–0.02	0.05	0.01	0.05	0.06
[Ti/Fe] _{TIH}	+0.02	–0.01	–0.02	–0.01	0.03	0.02	0.04	0.06
[V/Fe]	+0.03	+0.00	+0.03	–0.01	0.04	0.01	0.04	0.10
[Cr/Fe]	+0.02	–0.03	–0.01	–0.02	0.04	0.01	0.04	0.08
[Fe/H] _{FeI}	+0.07	+0.00	–0.02	–0.01	0.07	0.06	0.09	0.10
[Fe/H] _{FeII}	–0.02	+0.05	–0.02	+0.02	0.06	0.06	0.08	0.10
[Ni/Fe]	–0.01	+0.00	+0.01	+0.00	0.01	0.01	0.01	0.04
[Y/Fe]	+0.03	–0.01	–0.02	+0.00	0.04	0.01	0.04	0.27
[Zr/Fe]	+0.03	+0.00	+0.02	+0.00	0.04	0.01	0.04	0.23
[Ba/Fe]	+0.05	–0.01	–0.09	+0.00	0.10	0.03	0.10	0.23

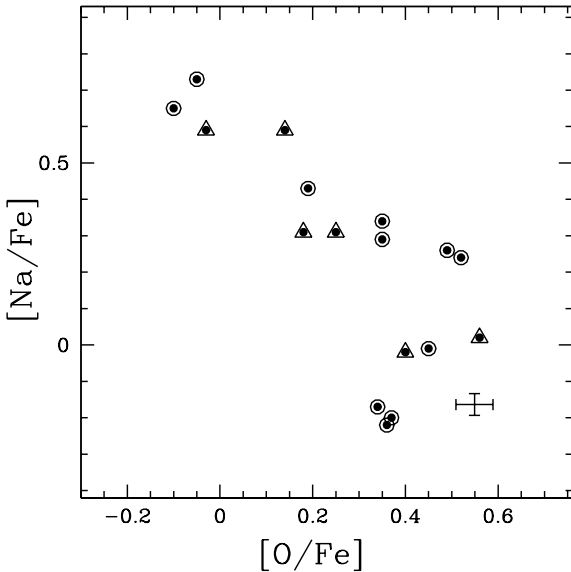


Fig. 3. The anti-correlation between [Na/Fe] and [O/Fe] abundance ratios. Triangles indicate stars that, on the basis of their position on the CMD, should be AGB.

compare the Na versus O trend for M 22 with those observed in other four GCs where multiple stellar populations have been identified: NGC 2808 (data from Carretta et al. 2006), NGC 1851 (data from Yong & Grundahl 2008), NGC 6388 (data from Carretta et al. 2007) and M 4 (data from Marino et al. 2008).

In NGC 2808 the presence of multiple stellar populations is inferred by the triple MS (Piotto et al. 2007). The three MS branches may be associated with the complexities of the cluster horizontal branch (D’Antona & Caloi 2004) and of its oxygen

abundance distribution (Carretta et al. 2006). On the contrary, the MS of M 22 is narrow and a spread or split, if any, must be smaller than 0.02 magnitudes in $m_{F435W} - m_{F814W}$ color (see Piotto 2009). Figure 4 shows that NGC 2808 stars cover almost the same range of Na abundances as M 22, but span a range of O abundance at least two times larger.

In M 4, the presence of multiple populations is inferred by the bimodal distribution of the Na abundance (Marino et al. 2008). In addition, stars from the two groups with different Na content populate two distinct RGB sequences in the U vs. $U-B$ CMD. Moreover, no MS or SGB split has been identified. Interestingly, in M 4, the maximum variations of [Na/Fe] and [O/Fe] are respectively 0.39 and 0.31 dex smaller than those observed in M 22. In particular, a few O-poor stars with $[O/Fe] < \sim 0.00$ and $[Na/Fe] > \sim 0.50$ are present among M 22 stars and lack in M 4.

As in M 22, in NGC 1851 (Milone et al. 2008) and NGC 6388 (Piotto 2008; Moretti et al. 2008; Piotto 2009) the presence of multiple populations is inferred by a split of the SGB. Unfortunately, for both these clusters, the available chemical measurements from high resolution spectroscopy are limited to seven RGB stars for NGC 6388 (Carretta et al. 2007) and eight RGB stars for NGC 1851 (Yong & Grundahl 2008). In the case of NGC 6388, the stars are located in a portion of the NaO plane that is not populated by any M 22 star of our sample, being NGC 6388 stars systematically O-poorer. On the contrary, the range of NaO anti-correlation in NGC 1851 matches quite well that of M 22.

At variance with the case of M 4 and NGC 2808, both NGC 1851 and M 22 seem to show a continuum distribution in [Na/Fe], without hints of multi-modalities, also if the small number of stars studied in this paper and in Yong & Grundahl (2008) for NGC 1851, prevents us from definitively excluding

the presence of discontinuities in the $[\text{Na}/\text{Fe}]$ or $[\text{O}/\text{Fe}]$ distribution.

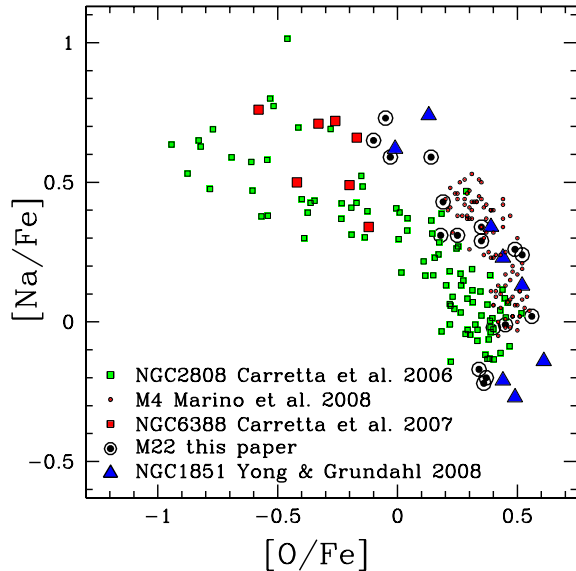


Fig. 4. NaO anti-correlation for M 22 stars superimposed to a collection of stars of four GCs that host multiple stellar populations.

4.3. Aluminum and Magnesium

The abundances of aluminum and magnesium have been determined from Al lines at 6696 Å, and 6698 Å, from the Mg doublet at 6318-6319 Å and the Mg line at 5711 Å.

Figure 5 shows the $[\text{Mg}/\text{Fe}]$ ratio as a function of $[\text{Al}/\text{Fe}]$. There is no clear MgAl correlation, despite of the presence of a well defined NaO anti-correlation, and of a clear AlNa correlation, as shown in Fig. 6. Assuming that Na enhancement comes from proton capture process at the expenses of Ne, we expect to observe also a MgAl anti-correlation, since Al forms at the expenses of Mg. This means we expect a decrease of Mg abundance with the increasing of Al content. We do not observe such an effect but, given our uncertainties, it could be too small to be detected. The lack of such a clear correlation was observed also in M 4 by Marino et al. (2008). However, they found a small difference in Mg content among stars characterized by large Na content differences, according to the scenario proposed by Ivans et al. (1999), who predicted that a drop of only 0.05 dex in Mg is needed to account for the increase in abundance of Al (see their Section 4.2.2).

4.4. *s*-process elements

We have measured abundance for three *s*-process elements: yttrium, zirconium, and barium. All of them span a wide range of abundance values. The maximum variations of $[\text{Y}/\text{Fe}]$, $[\text{Zr}/\text{Fe}]$ and $[\text{Ba}/\text{Fe}]$ have amplitudes of 0.87, 0.73 and 0.65 dex respec-

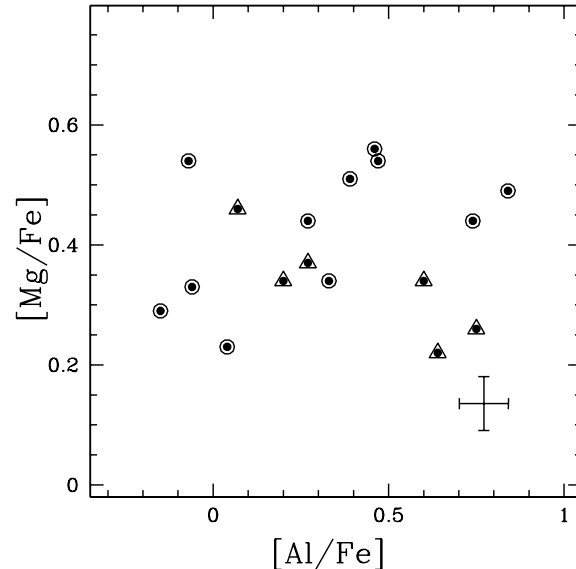


Fig. 5. $[\text{Mg}/\text{Fe}]$ vs. $[\text{Al}/\text{Fe}]$ abundance ratios.

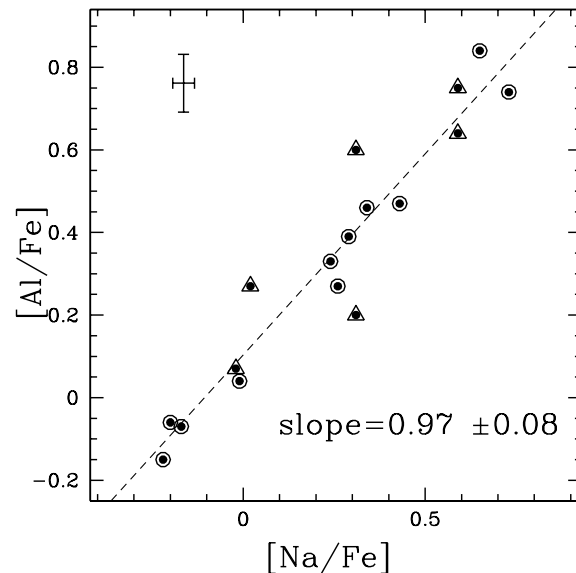


Fig. 6. $[\text{Al}/\text{Fe}]$ vs. $[\text{Na}/\text{Fe}]$ abundance ratios.

tively, despite of the small estimated internal error ($\sigma_{\text{tot}} \leq 0.1$, see Table 5).

In Fig. 7, we show $[\text{Zr}/\text{Fe}]$ and $[\text{Ba}/\text{Fe}]$ as a function of $[\text{Y}/\text{Fe}]$ (left and central panels), and $[\text{Ba}/\text{Fe}]$ as a function of $[\text{Zr}/\text{Fe}]$ (right panel). A clear correlation between each pair of *s*-process elements is evident, and also the slopes of the best fitting lines are similar.

Most importantly, the *s*-process elements clearly show a bimodal distribution: one group is overabundant in *s*-elements with average values of $[\text{Y}/\text{Fe}] = +0.34 \pm 0.05$, $[\text{Zr}/\text{Fe}] = +0.60 \pm 0.04$ and $[\text{Ba}/\text{Fe}] = +0.43 \pm 0.04$. This group contains seven out of seventeen stars (i.e. $\sim 40\%$ of the whole sample studied in this paper). The remaining ten

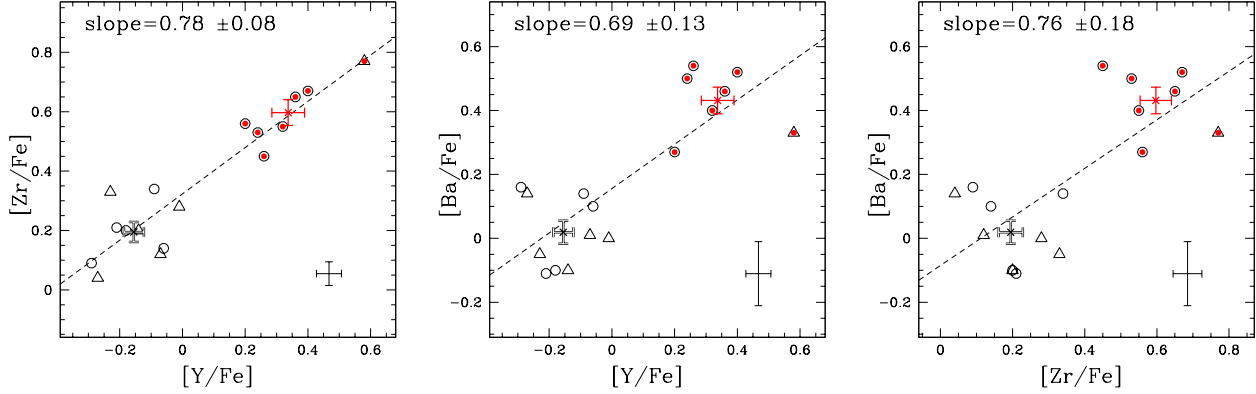


Fig. 7. From the left to the right: $[Zr/Fe]$ and $[Ba/Fe]$ vs. $[Y/Fe]$ and $[Ba/Fe]$ vs. $[Zr/Fe]$ abundance ratios. Stars rich in s -process elements are represented by red filled symbols, while s poor stars by the black empty ones. The red and the black crosses with error bars indicate the average abundances for stars of each group.

stars have $[Y/Fe] = -0.16 \pm 0.03$, $[Zr/Fe] = +0.20 \pm 0.03$, and $[Ba/Fe] = +0.02 \pm 0.04$.

Figure 7 suggests that we can isolate a s -process elements rich group, and a s -process elements poor one, by selecting stars with $[Y/Fe]$ greater and smaller than 0, respectively. Stars rich in s -process elements are represented by red filled symbols, while s poor stars by the black empty ones. Red and black crosses with error bars indicate the average abundances for stars of each group. In Table 6, we have listed the mean abundances for all the elements studied in this paper, calculated separately for each of these two groups. There are few remarkable differences in the average abundances for the two groups.

Table 6. Average abundances for s -element process poor and rich stars.

Element	s -process elements poor	s -process elements rich
[O/Fe]	0.30 ± 0.06	0.26 ± 0.10
[Na/Fe]	0.13 ± 0.11	0.40 ± 0.08
[Mg/Fe]	0.36 ± 0.04	0.45 ± 0.03
[Al/Fe]	0.26 ± 0.11	0.46 ± 0.10
[Si/Fe]	0.42 ± 0.01	0.44 ± 0.01
[Ca/Fe]	0.27 ± 0.01	0.38 ± 0.02
[Sc/Fe]	0.04 ± 0.02	0.04 ± 0.02
[Ti/Fe] _{TII}	0.22 ± 0.01	0.27 ± 0.03
[Ti/Fe] _{TIII}	0.33 ± 0.02	0.36 ± 0.03
[V/Fe]	-0.10 ± 0.04	-0.09 ± 0.03
[Cr/Fe]	-0.16 ± 0.02	-0.09 ± 0.04
[Fe/H]	-1.82 ± 0.02	-1.68 ± 0.02
[Ni/Fe]	-0.09 ± 0.01	-0.06 ± 0.01
[Y/Fe]	-0.16 ± 0.03	0.34 ± 0.05
[Zr/Fe]	0.20 ± 0.03	0.60 ± 0.04
[Ba/Fe]	0.02 ± 0.04	0.43 ± 0.04

As an example, in Fig. 8 we show the $[Y/Fe]$ ratio as a function of the $[Na/Fe]$, $[Al/Fe]$ and $[O/Fe]$ ratios. There is no clear correlation between Y, as well as Ba, and Zr abundances and Na, O or Al. However, stars enriched in s -process elements are all Na-rich and Al-rich, while the group of stars with lower

s -process elements abundance spans over almost all the values of Na and Al abundance.

The bi-modality in s -process elements in M 22 resembles the case of NGC 1851. In NGC 1851, Yong & Grundahl (2008) noted that the abundances of the s -process elements Zr and La appear to cluster around two distinct values. They suggested that the two corresponding groups of stars should be related to the two stellar populations photometrically observed by Milone et al. (2008) along the SGB. In NGC 1851 the s -element abundance appears also to correlate with Na, Al and O abundance.

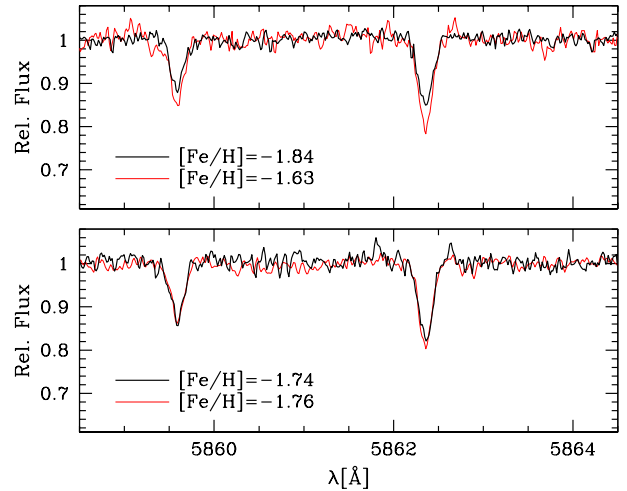


Fig. 9. The upper panel shows the spectra of the metal poor stars #200068 ($[Fe/H] = -1.84$) and of the metal rich star #200083 ($[Fe/H] = -1.63$) centered on the lines of FeI. The stellar parameters are very similar, however, the Fe lines differ significantly. The bottom panel shows the same lines for stars #200101 and #71 with similar metallicity and stellar parameters.

By the similarity between our results and the ones by Yong & Grundahl (2008) on NGC 1851, it is tempting to associate the presence of the two groups of stars with different s -process

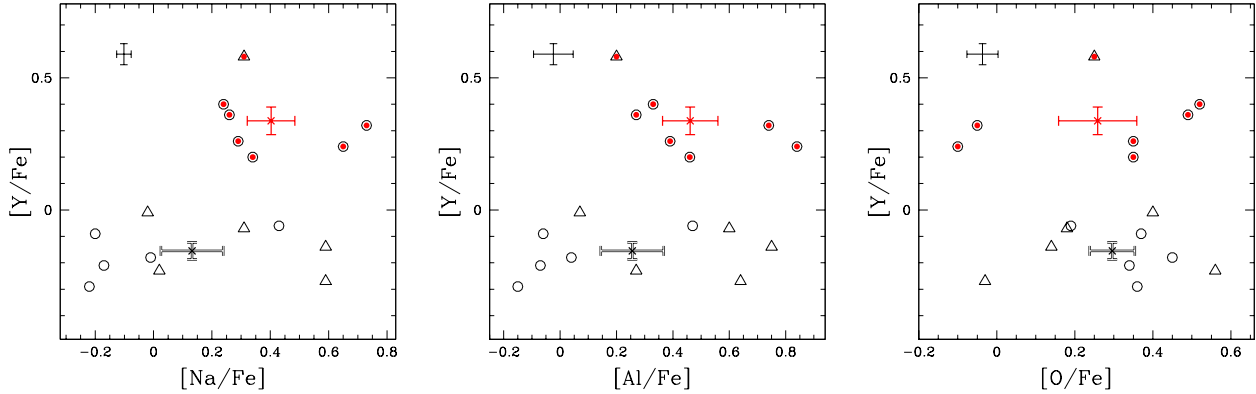


Fig. 8. From the left to the right: [Y/Fe] as a function of [Na/Fe], [Al/Fe] and [O/Fe] abundance ratios. Symbols are as in Fig. 7.

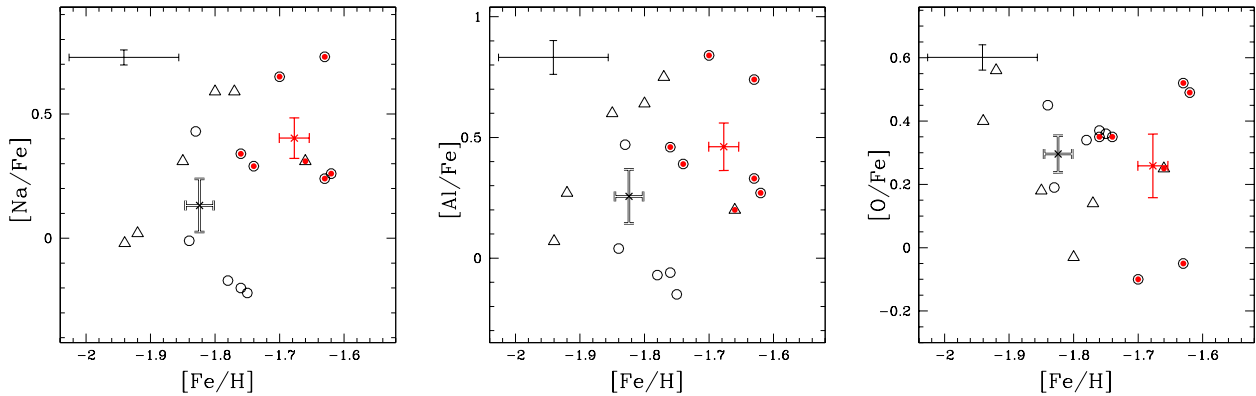


Fig. 10. From the left to the right: [Na/Fe], [Al/Fe] and [O/Fe] as a function of [Fe/H] abundance ratios. Symbols are as in Fig. 7.

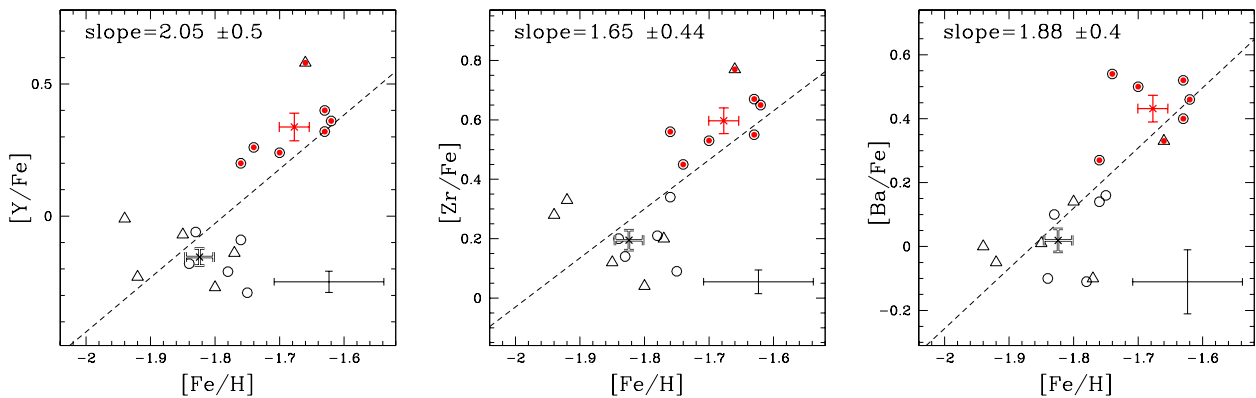


Fig. 11. [Y/Fe] (*left*), [Zr/Fe] (*center*) and [Ba/Fe] (*right*) as a function of [Fe/H]. Symbols are as in Fig. 7, dashed lines are the best least square fitting straight lines.

element content, with the two populations of stars isolated along the SGB of M 22 by Piotto (2009, see also Fig.18). Note that barium, yttrium, and zirconium can be considered as the signature of the *s*-process that occurs in intermediate mass AGB stars (Busso et al. 2001), whose wind could have polluted the primordial material from which the second generation of stars in M 22 and NGC 1851 formed. Also the fact that *s*-element rich stars seem to be also rich in Na and Al could

be due to the pollution from intermediate mass AGB stars of the material from which a second generation of stars formed, though the lack of a clear correlation is more difficult to interpret.

We note that also the results by Piotto et al. (2005) on the metal content of the stars in the two main MSs of ω Centauri can be interpreted within this scenario. Piotto et al. (2005) found [Ba/Fe] \sim 0.5 for the metal-poorer ([Fe/H] \sim -1.68) red

MS, and $[\text{Ba}/\text{Fe}] \sim 0.8$ for the metal-richer ($[\text{Fe}/\text{H}] = -1.37$) bluer MS. This result was further confirmed by Villanova et al. (2007), who observed that SGB metal-poor stars have a Ba content lower than intermediate-metallicity ones by about 0.2 dex.

The relations between the s -process element abundance and the iron content in M 22 is the argument of the following section.

5. The spread in Fe of M 22

As discussed in Section 1, for long time, the existence of an intrinsic Fe spread in M 22 has been debated in the literature (see Ivans et al. 2004 for a review), since photometric and spectroscopic studies have yielded conflicting results. Some spectroscopic studies found no significant variations (Gratton 1982, Ivans et al. 2004), whereas others seem to find a variation in $[\text{Fe}/\text{H}]$ up to ~ 0.5 dex (Pilachowsky et al. 1984). Photometric studies gave similar controversial results. Undoubtedly, the RGB of M 22 has a large spread in color. This spread is observed both in BVI and Strömgren photometry, but interpreted either in terms of metallicity variation or differential reddening, or a combination of the two.

We want to emphasize again that the $[\text{Fe}/\text{H}]$ measurements presented in this paper are not based on photometric data, and therefore do not suffer the effects of differential reddening. For this reason, they constitute an appropriate tool to make the issue of $[\text{Fe}/\text{H}]$ variations in M 22 clearer.

From Table 5, we see that the observed dispersion σ_{obs} in iron is comparable with the estimated internal error σ_{tot} , i.e. the observed star-to-star metallicity scatter could be interpreted as due to measurement errors only. This fact demonstrates how difficult it is to establish the statistical significance of any intrinsic spread in $[\text{Fe}/\text{H}]$. In this paper, we can tackle the problem of the iron dispersion in M 22 in a different way. The observed dispersion in iron content alone could be a poor indicator of any intrinsic metallicity dispersion. First of all, because of the abundance measurements errors. In addition, we note that if anomalies in $[\text{Fe}/\text{H}]$ affect only a small fraction of M 22 stars, their effect on the iron dispersion of the whole sample of stars could result to be negligible.

A visual inspection of some spectra reinforces the suggestion that there may be star-to-star iron variations. As an example, in Fig. 9, we show spectra of two pairs of stars with very similar stellar atmospheric parameters. The two spectral lines in Fig. 9 are iron lines. The upper panel shows the spectra of the stars #200068 and #200083 for which we have measured an iron abundance $[\text{Fe}/\text{H}] = -1.84$ and $[\text{Fe}/\text{H}] = -1.63$, respectively (see Table 3). The line depths differ significantly and, because of the similarity in the atmospheric parameter, must indicate an intrinsic iron difference. As a comparison, in the bottom panel we plot the same spectral region for two stars (#200101 and #71) with almost the same iron content.

Our results on the iron dispersion can not be conclusive by themselves. However, it is rather instructive to look for possible correlations between $[\text{Fe}/\text{H}]$ and the other chemical abundances (mainly the ones showing a spread or bimodal distribution, as the s -process elements).

Figure 10 shows that Fe abundance is not significantly correlated with the Al, Na, and O abundances, elements which, on the other hand, are involved in a well defined anti-correlation, as discussed in Section 4.2.

However, when we compare the iron abundances with the s -process element abundances, we find a strong correlation, with s -process element rich stars having systematically higher $[\text{Fe}/\text{H}]$, as shown in the three panels of Fig. 11. The two s -process element rich and poor groups have average $[\text{Fe}/\text{H}]_{s\text{-rich}} = -1.68 \pm 0.02$ and $[\text{Fe}/\text{H}]_{s\text{-poor}} = -1.82 \pm 0.02$, respectively ($\delta [\text{Fe}/\text{H}] = 0.14 \pm 0.03$).

We want to emphasize that the significance in the Fe variation can be appreciated only when we consider the average iron content of the two groups characterized by a different s -elements content. This is further demonstrated by a simple test we run, and whose results are summarized in Fig. 12. We simulated 100,000 stars with iron content, and iron abundance dispersion as the observed stars, i. e. 41% of the sample are s -process element rich stars (red Gaussian) and a 59% are s -process element poor ones (blue Gaussian) with a mean $[\text{Fe}/\text{H}]$ of -1.82 and -1.68 dex, respectively. The dispersion in iron content of each group was taken equal to 0.09 dex, that is the error we estimated for the iron abundance (see Table 5). The resulting metallicity abundance dispersion for the total sample is of 0.11 dex, which is close to, and only marginally greater, than the dispersion expected from the measurement errors.

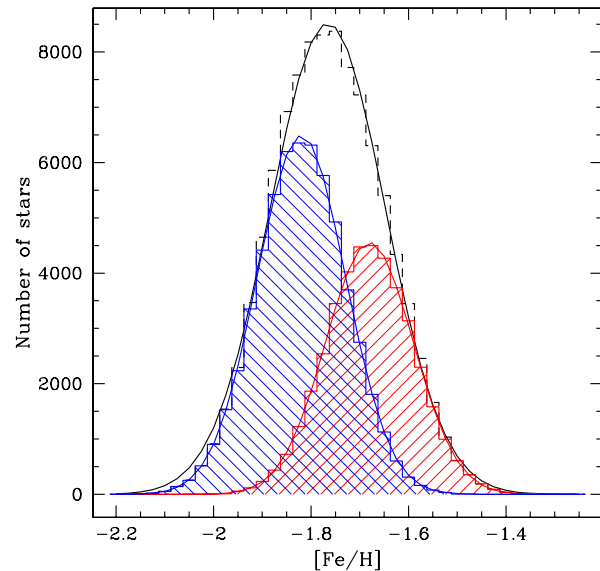


Fig. 12. Simulation of 100,000 stars with the properties of the two observed groups of stars. The red and the blue histograms represent the s -rich and the s -poor groups of stars respectively.

The presence of two groups of stars, one of which enriched both in s -process elements and iron, is analogous to the case of ω Centauri discussed in the previous Section 4.4, where Piotto et al. (2005) and Villanova et al. (2007) found that the more metal rich, He-enriched stars have also higher Ba content.

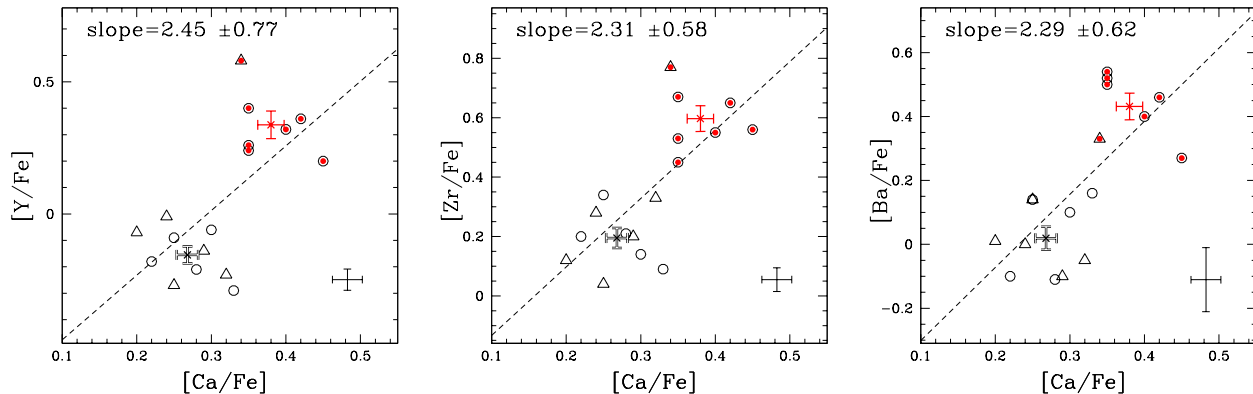


Fig. 14. $[Y/Fe]$ (left), $[Zr/Fe]$ (center) and $[Ba/Fe]$ (right) as a function of $[Ca/Fe]$. Symbols are as in Fig. 7, dashed lines are the best least square fitting straight lines.

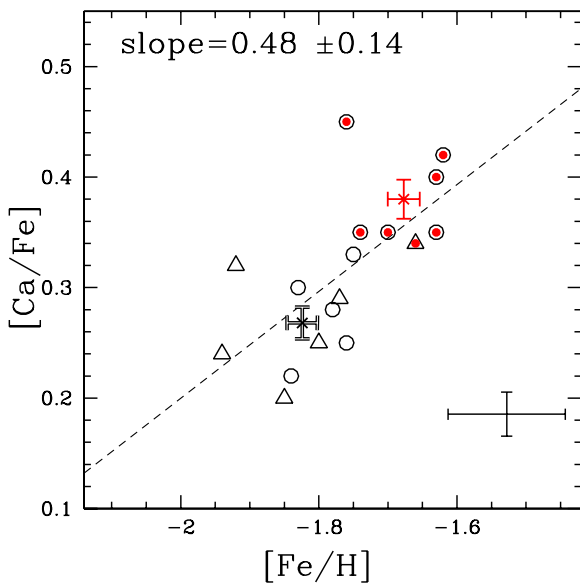


Fig. 13. $[Ca/Fe]$ as a function $[Fe/H]$.

As shown in Fig. 13, the iron abundances are well correlated also with calcium abundances, and the Ca content correlates with the s -process element abundance. Again, a similar behavior is present in ω Centauri, where a spread in Ca was known since Freeman & Rodgers (1975). More recently, Villanova et al. (2007) showed that the SGB population with $[Fe/H] \sim -1.2$ has a mean $[Ca/Fe]$ larger by ~ 0.1 dex, than that found in the more metal-poor population.

In M 22, evidence for a calcium spread was already noted and Norris & Freeman (1983) showed a correlation between CN variations and Ca, similar to those in ω Centauri. Lehnert et al. (1991), by studying a sample of 4 stars, found both Ca and Fe variations correlated with the CN-band strengths.

Our abundance measurements show that both calcium and iron correlate with the s -process elements (Fig. 14 and Fig. 11). Moreover, as shown in Fig. 15, we found that calcium, like

iron, is not clearly correlated with Na, although the stars with an higher Ca content seem to be slightly Na rich.

In Fig. 7, Fig. 11, Fig. 13, and Fig 14 six out of seven probable AGB stars, represented by triangles, belong to the s -poor group. We want to emphasize here that our selection of the probable AGB stars is based only on a visual inspection of the stars on the CMD, without considering photometric errors. In any case, assuming that all these stars are indeed real AGB members, our s -poor sample would include both RGB and AGB stars. If in our s -poor sample there is really a group of AGB stars, they could be the evolution of low mass stars of the primordial population, not able to activate the third dredge-up and enrich their surface of s -process elements. Hence they should trace the primordial composition of the cluster. Possibly, due to the larger iron content, stars with higher s element content, have systematically redder colors with respect s -process element poor stars, and have low probability to be pushed by photometric errors in to the AGB region.

Figure 16 shows $[Mg/Fe]$ and $[Si/Fe]$ as a function of $[Fe/H]$. Both Mg and Si are slightly overabundant in s -process element rich stars with respect to s -process element poor ones (see also Table 6). This seems to suggest that core collapse SNe (CCSNe) are the best candidates to produce the iron excess of the second generation of stars. Indeed, would iron be produced by Type Ia SNe, we would expect a lower $[Mg/Fe]$ and $[Si/Fe]$ ratio for the group of stars enriched in s -process elements with respect to the first generation of (s -process element poor) stars. In fact, SNeIa events are selectively enriched in iron (although modest quantity of Si are also produced). On the contrary, CCSNe along with iron, produce also Mg and Si in higher quantity with respect to SNeIa.

With a present day mass of $\sim 5 \times 10^5 M_{\odot}$ (Pryor & Meylan 1993) NGC 6656 is one of the most massive GCs of the Milky Way. The s -elements rich population, with a mass of $\sim 2 \times 10^5 M_{\odot}$ and an iron abundance $[Fe/H] = -1.68 \pm 0.02$ dex, includes $\sim 1.5 M_{\odot}$ of fresh iron if we assume $Z_{\text{Fe}}^{\text{Fe}} = 0.0013$. On average each CCSN produces $\sim 0.07 M_{\odot}$ of iron (Hamuy 2003), therefore about twenty SNe are needed to produce the fresh iron of the second stellar population. In this scenario, the fainter SGB

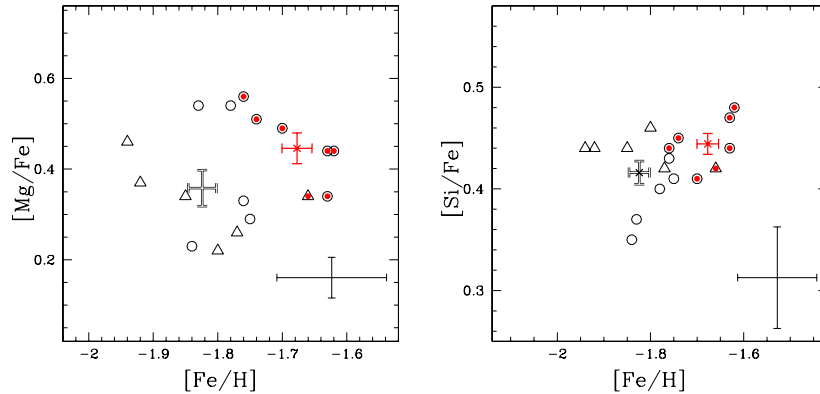


Fig. 16. $[Mg/Fe]$ (left), and $[Si/Fe]$ (right) as a function of $[Fe/H]$. Symbols are as in Fig. 7.

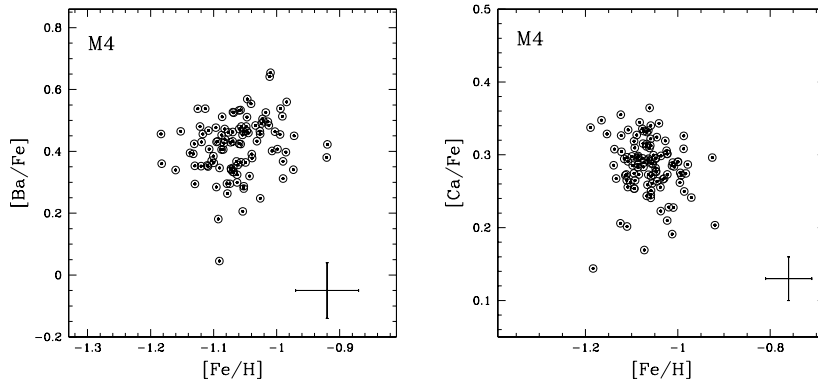


Fig. 17. $[Ba/Fe]$ (left), and $[Ca/Fe]$ as a function $[Fe/H]$ (right) for 104 stars in the GC M 4 (from Marino et al. 2008).

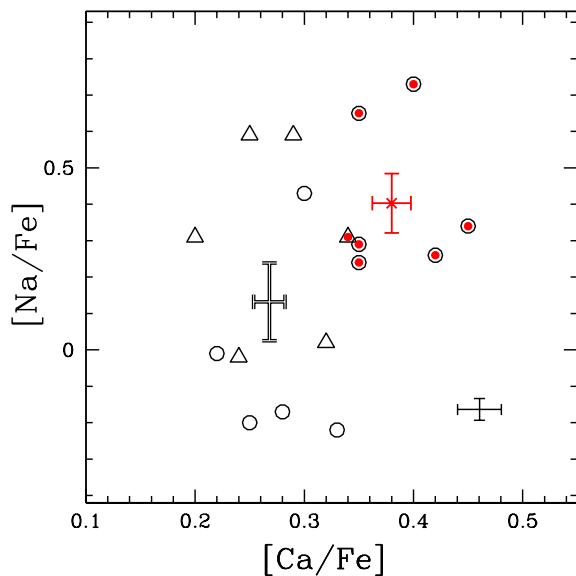


Fig. 15. $[Na/Fe]$ as a function of $[Ca/Fe]$. Symbols are as in Fig. 7.

(and TO) of this second generation of stars is attributed to their different chemical mixture, rather than to an age difference.

6. Can the iron spread account for the SGB split?

Figure 18 from Piotto (2009) shows that the SGB of M 22 is splitted into two branches. In the previous section, we have shown that in M 22 there are two groups of stars, with different s -process element contents, and with two different average iron contents. In this section, we want to investigate whether the different iron content can explain the split of the SGB.

In Fig. 19, we compare two isochrones from Pietrinferni et al. (2004) in the ACS/WFC plane m_{F606W} vs. $m_{F606W} - m_{F814W}$ of Fig. 18. Both of them have an age of 14 Gyr, but different metallicities. The black line corresponds to the mean metallicity of the group of s -process element poor stars ($[Fe/H] = -1.82$) and the dashed red line is an isochrone with the average $[Fe/H] = -1.68$ of the s -process element rich stars. The different metallicity mainly reflects in a split of the RGB and of the SGB. In the inset, we show a zoom of the SGB region. At $m_{F606W} - m_{F814W} = 0.85$ the difference in magnitude m_{F606W} between the two isochrones is $\delta m_{F606W} = 0.10$, about 0.07 magnitudes smaller than that observed by Piotto (2009). We conclude that the observed difference in $[Fe/H]$ can contribute to produce the splitting of the SGB observed by Piotto (2009), but it is not sufficient. On the other hand, the entire shape of the turn off-SGB-RGB region is difficult to reproduce with standard, alpha-enhanced isochrones. Likely, this is due to the fact that the origin of the split may be much more complicated and

involves also the NaCNO abundances, as suggested by Cassisi et al. (2008) for the case of NGC 1851.

7. Comparison with M 4

In this section, we present a comparative analysis between the chemical abundances obtained in this paper for M 22 and the abundance measurements on M 4 RGB stars by Marino et al. (2008) to better outline the complexity of the multiple population appearance in different clusters.

Such a comparison is rather instructive. First of all, because M 4, similarly to M 22, is affected by high differential reddening (Lyons et al. 1995, Ivans et al. 1999), and moreover, their spectra were analysed employing the same procedure. We note also that the UVES spectra of M 4 were collected with the same set-up and have almost the same S/N ratio as the M 22 spectra analysed in this work.

Marino et al. (2008) have shown that M 4 hosts two distinct stellar populations, characterized by different Na content, and different CN-band strength. These two groups of stars also define two sequences along the RGB, but there is no SGB split. At variance with M 22, M 4 does not show any evidence of intrinsic Fe spread. Marino et al. (2008) set an upper limit for the $[\text{Fe}/\text{H}]$ spread of 0.05 dex (1σ) in M 4. In the case of M 22, as discussed in Section 4.2, we identified a well defined NaO anticorrelation, but we have no evidence of a dichotomy in Na distribution, as in M 4. Instead, we found a dichotomy in the s -process elements, and the SGB is splitted into two branches.

As a comparison, we show in Fig.17 the Fe abundances as a function of Ba and Ca in M 4, using the same scale used for the same plot for our M 22 targets (Fig. 11, right panel, and Fig. 13 respectively). In the case of M 4 there is no evidence of a chemical spread in $[\text{Ba}/\text{Fe}]$ vs. $[\text{Fe}/\text{H}]$ nor in $[\text{Ca}/\text{Fe}]$ vs. $[\text{Fe}/\text{H}]$. Note that the rms of the calcium abundance in M 4 is 0.04 dex, to be compared with the $\sigma_{\text{obs}} = 0.07$ (see Table 5) we found for the same element in M 22. We find a rms in the calcium abundance almost equal to the one found in M 4 when we divide our stellar sample into the two s -process element rich and poor groups ($\sigma_{\text{obs}} = 0.04$ for both the two s groups).

Apparently, the two stellar populations in M 4 and M 22 have different origin, or the mechanisms responsible for this dichotomy must have been acting with different intensities in the two clusters.

8. An independent check of the results

In this paper we have presented a clear evidence of a spread in $[\text{Fe}/\text{H}]$ and of the presence of a bimodal distribution in s -process element content among the M 22 stars. These results are based on high resolution UVES spectra of seventeen stars. Because of the high relevance of these results in the context of the ongoing lively debate on the multipopulation phenomenon in star clusters, we further searched in the ESO archive for additional spectra of M 22 stars in order to strengthen the statistical significance of the results from UVES data. In fact, we found GIRAFFE spectra for 121 stars. We reduced all of them, but only fourteen were in the appropriate RGB location to have high enough S/N to pass all of our quality checks (see the

following discussion) and useful for the abundance measurements. In any case we could double the original UVES sample of stars.

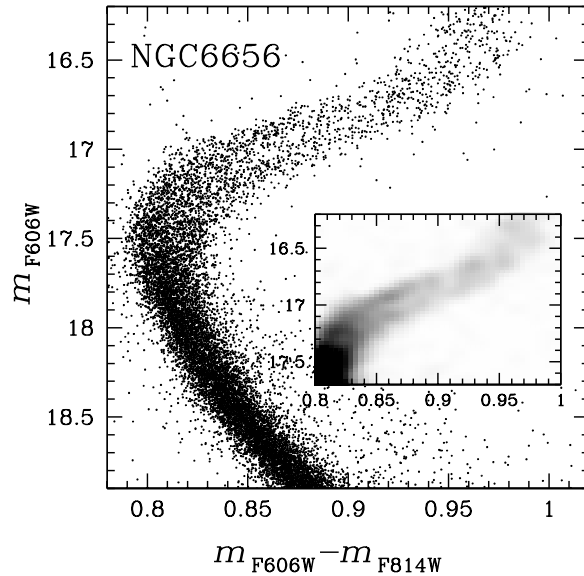


Fig. 18. ACS/WFC CMD of M 22 from Piotto (2009).

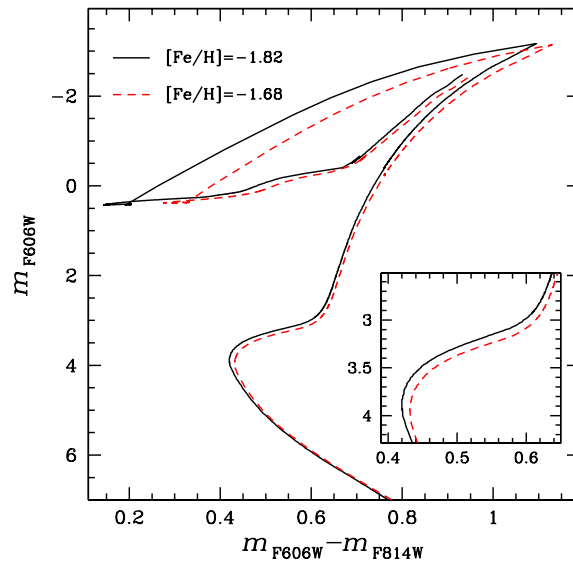


Fig. 19. Red and blue lines are theoretical isochrones from Pietrinferni et al. (2004), with $[\text{Fe}/\text{H}] = -1.68$ and $[\text{Fe}/\text{H}] = -1.82$. The difference in metallicity produces on the CMD a split of the RGB and the SGB.

Each star was observed with HR09, HR13, and HR15 set-ups, which give a resolution of about $R \sim 20000$ - 25000 in 514-535, 612-640, and 660-696 nm respectively. Data were reduced using the last version of the pipeline developed by

Geneva observatory (Blecha et al. 2000), and were bias-subtracted, flat-field corrected, and extracted applying a wavelength calibrations obtained by ThAr lamps. Each spectrum was then normalized. Finally for each star we obtained radial velocity and applied a membership criterion as done for UVES data. Spectra of each member star were then reported to rest-frame velocity and combined together. We performed also a test in order to verify the influence of scattered light on the spectral line shape (and could alter the final abundances). To this aim we reduced some spectra covering the whole GIRAFFE CCD with and without scattered-light subtraction and compared spectral features. We found that scattered-light has no significant influence on lines.

For GIRAFFE data analysis, we wanted to follow the same procedure used for UVES, i.e. obtaining atmospheric parameters only from spectroscopy and not from photometry, which can be altered by differential reddening. This approach has the advantage to put the abundance determinations from the two data-sets in the same abundance scale, avoiding systematic effects. However, this choice, coupled with the selection of stars located only in the RGB, was paid by the rejection of 103 spectra because of their low S/N ($\leq 70-80$). Indeed an high S/N ratio is necessary to measure a sufficient number of isolated FeI/II lines in GIRAFFE spectra, which have lower resolution and cover a smaller wavelength range with respect to UVES ones. In addition, the brightest stars were not analyzed because of their very low temperature ($T_{\text{eff}} < 4000$). In this T_{eff} regime also metal poor stars (as in the case of M 22) show very strong lines, which are blended in GIRAFFE data, not allowing a reliable EW measurement.

After a star passed through our selection criteria, atmospheric parameters (and Fe content) were obtained by EW method, as done for UVES and using the same line-list for the spectral lines in common between the two set-ups.

Because of the two different data-sets, some comparisons are needed between the results obtained from the two spectrographs. Since we have only one star (#51) in common between the two data-sets, we could not compare directly (apart for this star) the results. In Tab. 7 we list the chemical abundances in common obtained for this star from the two different data. We note that the atmospheric parameters are in agreement within the errors calculated for UVES, the values for Fe and Y abundances are within the σ_{tot} listed in Tab. 5, while for the other elements there are larger discrepancies probably due to errors associated to GIRAFFE results (that we have not considered here). Since the comparison of one star is not enough to verify the compatibility between the two set of abundances, we compared the atmospheric parameters and the mean metallicity.

Figure 20 summarizes our tests. Filled circles represent GIRAFFE results, while open squares the UVES ones. In the upper left panel we plotted $\log(g)$ vs. T_{eff} , while the upper right panel shows v_t vs. $\log(g)$. Both gravity as a function of temperature and microturbulence velocity as a function of gravity follow the same general trend for the two data-sets, with similar dispersions. Further tests are shown in the two lower panels. The lower left one shows the Fe abundance vs. V magnitude (i.e. vs. the evolutionary state of the star along the RGB). No correlation appears, meaning that no systematic errors due to

the different evolutionary phase are presents. The lower right panel reports T_{eff} vs. $B - V$ color. The line is the empirical relation by Alonso et al. (1999), obtained assuming a reddening $E(B - V) = 0.34$ (Harris 1996). Also in this case a good agreement was found, not only for the zero-point of the relations (i.e. the absolute average reddening of the cluster), but also for the shape of the relations themselves.

An important test comes from the comparison of the mean iron content obtained from the two data-sets. From the fourteen GIRAFFE stars, we obtain:

$$\langle [\text{Fe}/\text{H}] \rangle = -1.74 \pm 0.03$$

which perfectly agrees with the UVES value within 1σ .

A rough estimate of errors on atmospheric parameters can be done as in Marino et al. (2008), assuming that stars with the same V magnitude (corrected for differential reddening) have the same parameters. In this way we can obtain an upper (also the dispersion in metal content can in part contribute to the dispersion of the stellar parameter values at a given luminosity along the RGB) estimate of the errors, which are $\Delta T_{\text{eff}} = \pm 65$ K, $\Delta \log(g) = \pm 0.20$, and $\Delta v_t = \pm 0.11$ km/s respectively. We can see that errors are a bit larger, but still comparable with UVES ones.

All the other elements, with the exception of Ti, in GIRAFFE data were measured by spectral synthesis because of the severe blends with other lines. In addition to Fe and Ti we measured O (from the forbidden line at 630 nm), Na (from the doublet at 615 nm), Y (from the doublet at 520 nm), Ba (from the line at 614 nm), Nd (from the line at 532 nm), and Eu (from the line at 665 nm).

Having verified the good agreement between the atmospheric parameters and the iron content obtained from the two data-sets, we can further proceed to verify whether GIRAFFE data confirms UVES results. For this reason, in Fig. 21 we show some of the trends discussed in the previous sections. Filled circles are GIRAFFE measurements, while open circles are UVES ones. It is clear from this comparison that UVES results are fully confirmed. In particular, we can confirm the Y-Ba bimodality (central panel), as well as the different Fe content for the two s -element rich and s -element poor groups of stars (see leftmost and rightmost middle panels).

In addition, from GIRAFFE data we measured also Nd (a combined s and r element) and Eu (a pure r element) lines. Their abundances as a function of $[\text{Fe}/\text{H}]$ are shown in the central and right lower panels. There is no trend for $[\text{Eu}/\text{Fe}]$, while $[\text{Nd}/\text{Fe}]$ clearly correlates with $[\text{Fe}/\text{H}]$. This is a further evidence that the iron enrichment of the s -process rich group is due to core-collapse SNe.

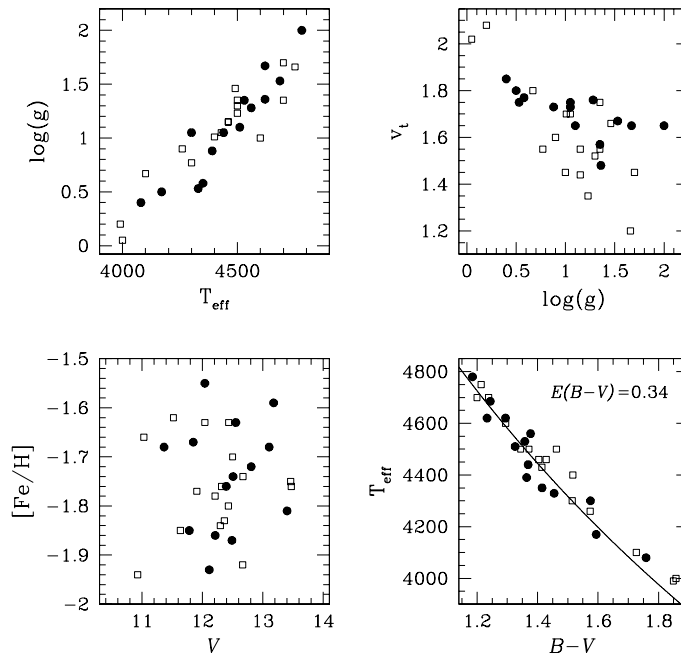
9. Two stellar populations in M 22

In the present paper we presented high resolution spectroscopic analysis for a sample of seventeen RGB stars in the GC M 22 from UVES and FLAMES+UVES data.

We confirm that M 22 is a metal poor GC, with a mean iron-content $[\text{Fe}/\text{H}] = -1.75 \pm 0.02$ (weighted mean between UVES and GIRAFFE) and a mean α -enhancement

Table 7. Atmospheric parameters and chemical abundances for the star #51 obtained from UVES and GIRAFFE data.

	T_{eff} [K]	$\log(g)$	v_t [km s $^{-1}$]	[Fe/H]	[O/Fe]	[Na/Fe]	[Ti/Fe]	[Ni/Fe]	[Y/Fe]	[Ba/H]
UVES	4260	0.90	1.60	-1.63	-0.05	0.74	0.23	-0.07	0.32	0.40
GIRAFFE	4300	1.05	1.75	-1.55	0.05	0.60	0.38	-0.18	0.29	0.59

**Fig. 20.** Check of the atmospheric parameters used in this paper. Filled circles are GIRAFFE stars, while open squares are UVES ones. See Section 8 for a full explanation.

$[\alpha/\text{Fe}] = +0.36 \pm 0.04$. Sodium and oxygen follow the well known anti-correlation, while no evidence for an Mg-Al anticorrelation was revealed. A clear correlation was found between Na and Al.

We find a strong dichotomy in the distribution of the s -process elements barium, yttrium and zirconium. Most importantly, we find that the abundance of these elements is correlated with the iron abundance. Stars enriched in s -process elements also show larger values of $[\text{Fe}/\text{H}]$, by ~ 0.14 dex. The s -process elements abundance correlates with calcium, and calcium with iron. No clear correlation is present between s -process elements and sodium, and between iron and sodium, but we noted that s -element and Fe enriched stars show higher values of sodium. These stars show also an overabundance of magnesium and silicon. The correlation between s -process elements, and Ca abundances, with $[\text{Fe}/\text{H}]$ is the strongest argument in favor of the presence of two groups of stars with a different Fe content in M 22. All these results have been confirmed by a sample of fourteen lower resolution GIRAFFE spectra, which allowed us to double the original UVES sample.

According to the most recent theoretical models by Pietrinferni et al. (2004), a difference in metallicity of 0.14 dex should cause a difference of ~ 0.10 mag in the F606W ACS/WFC band at the level of the SGB. Piotto (2009) have in-

deed found that the SGB of M 22 is separated into two, distinct branches. However, the average separation in F606W band is of 0.17 magnitudes: it appears that the SGB split can not be attributed to a difference in $[\text{Fe}/\text{H}]$ alone.

The fraction of stars on the bright SGB (bSGB) corresponds to $62\% \pm 5\%$ of the total SGB population, while the faint SGB (fSGB) includes the remaining $38\% \pm 5\%$ of the SGB stars (Piotto 2009). In the stellar sample of the present paper, the fraction of Ba-strong, Y-strong, Zr-strong stars is $\sim 41\%$. It is therefore tempting to connect the s -process element poor sample to the bright SGB stars, while the faint SGB stars could be the ones with enhanced s -process elements. The correct reproduction of the two SGBs needs an accurate determination of the NaCNO abundances, as shown by Cassisi et al. (2008) for the analogous case of NGC 1851. Also an He variations between the two populations can affect the SGB morphology. Indeed, we note that M 22 shares similarities with ω Centauri and NGC 1851: these clusters, where multiple stellar populations have been photometrically identified along the SGB, exhibit a large range, not only in C, N, O, Na, Al, but also in s -process element abundance. M 22 is the only globular, apart ω Centauri, where some evidence of an intrinsic spread in iron were observed. Some hints (even if very uncertain due to the low number statistics of the analyzed sample) for a some

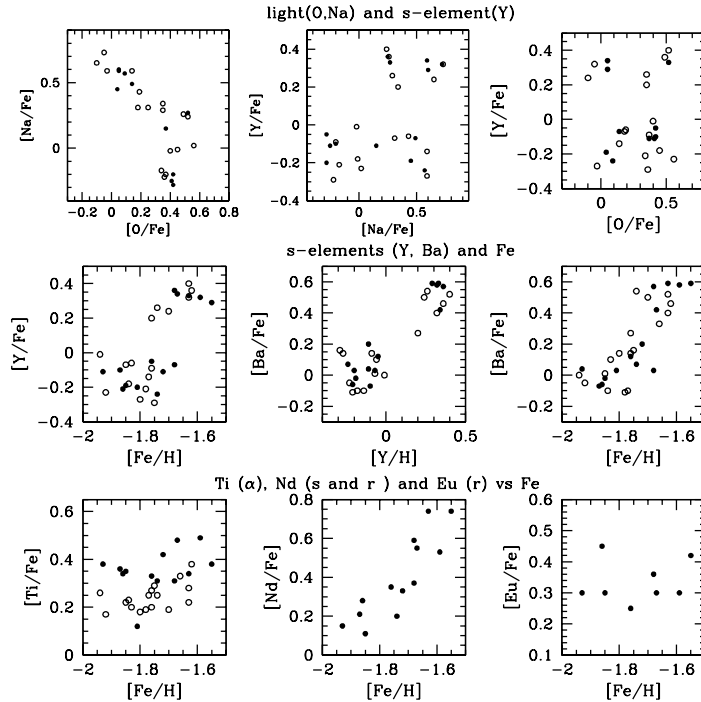


Fig. 21. Comparison of our final results we obtained for UVES (open circles) and GIRAFFE (filled circles).

iron spread in NGC 1851 was suggested by Yong & Grundahl (2008). NGC 1851, ω Centauri, and M 22 show a large variation in the Strömgen index, traditionally used as a metallicity indicator. All of these three GCs have a splitted SGB.

From our observations and from the results of Piotto (2009), it is tempting to speculate that the SGB split could be related to the presence of two groups of stars with different s -process element content and a difference, albeit small, in iron. According with this scenario, s -process element poor stars are those populating brighter SGB stars and constitute the first M 22 population. The second stellar generation should have been formed after that the AGB winds of this first stellar generation have polluted the protocluster interstellar medium with s -process elements. This second generation may have formed from material which was also enriched by core-collapse supernovae ejecta, as indicated by the higher iron, magnesium, and silicon content, and the lack of correlation of the iron content with a pure r -process element (Eu). A detailed analysis of the C, N, O abundances of the SGB stars in M 22 is strongly needed in order to properly settle this problem.

Acknowledgements. We warmly thank the referee, J. Cohen, for her comments and suggestions which surely helped to strengthen the results presented in this paper. We also thank P. Marigo for useful discussion. AFM, APM, AB, AR, and GP acknowledge the support by the MIUR-PRIN2007 prot. 20075TP5K9. AFM acknowledges partial support by Fondazione A. Gini. APM acknowledges partial support by ASI. A.B. acknowledges the support of the CA.RI.PA.RO. foundation, and the STScI under the 2008 graduate research assistantship program.

References

- Alonso, A., Arribas, S., & Martinez-Roger, C. 1999, *A&A*, 140, 261
 Ballester, P., Modigliani, A., Boitquin, O., et al. 2000, *ESO Messenger*, 101, 31
 Bellini, A., et al. 2009, *A&A*, 493, 959
 Bedin, L. R., Piotto, G., Anderson, J., Cassisi, S., King, I. R., Momany, Y., & Carraro, G., 2004, *ApJ*, 605, L125
 Blecha, A., Cayatte, V., North, P., Royer, F., & Simond, G. 2000, *Proc. SPIE*, 4008, 467
 Brown, J. A., & Wallerstein, G. 1992, *AJ*, 104, 1818
 Busso, M., Gallino, R., Lambert, D. L., Travaglio, C., & Smith, V. V. 2001, *ApJ*, 557, 802
 Cannon, R. D., Croke, B. F. W., Bell, R. A., Hesser, J. E., & Stathakis, R. A. 1998, *MNRAS*, 298, 601
 Carretta, E., Gratton, R. G., Lucatello, S., Bragaglia, A., & Bonifacio, P. 2005, *A&A*, 433, 597
 Carretta, E., Bragaglia, A., Gratton, R. G., Leone, F., Recio-Blanco, A., & Lucatello, S. 2006, *A&A*, 450, 523
 Carretta, E. et al., 2007, *A&A*, 464, 967
 Carretta, E., Bragaglia, A., Gratton, R. G., & Lucatello, S. 2008, arXiv:0811.3591
 Cassisi, S., Salaris, M., Pietrinferni, A., Piotto, G., Milone, A. P., Bedin, L. R., & Anderson, J. 2008, *ApJ*, 672, L115
 Cohen, J. G. 1981, *ApJ*, 247, 869
 Cohen, J. G., & Meléndez, J. 2005, *AJ*, 129, 303
 D’Antona, F., & Caloi, V. 2004, *ApJ*, 611, 871
 Dekker, H., D’Odorico, S., Kaufer, A., Delabre, B., & Kotzlowski, H. 2000, *Proc. SPIE*, 4008, 534
 Freeman, K. C., & Rodgers, A. W. 1975, *ApJ*, 201, L71
 Gratton, R. G. 1982, *A&A*, 115, 171
 Gratton, R. G., et al. 2001, *A&A*, 369, 87
 Gratton, R., Sneden, C., & Carretta, E. 2004, *ARA&A*, 42, 385
 Hamuy, M. 2003, *ApJ*, 582, 905
 Harris, W. E. 1996, *VizieR Online Data Catalog*, 7195, 0

- Hesser, J. E., Hartwick, F. D. A. & McClure, R. D. 1977, *ApJS*, 33, 471
- Ivans, I. I., Sneden, C., Kraft, R. P., Suntzeff, N. P., Smith, V. V., Langer, G. E., & Fulbright, J. P. 1999, *ApJ*, 118, 1273
- Ivans, I. I., Sneden, C., Wallerstein, G., Kraft, R. P., Norris, J. E., Fulbright, J. P., & Gonzalez, G. 2004, *Memorie della Societa Astronomica Italiana*, 75, 286
- Kaysner, A., Hilker, M., Grebel, E. K., & Willemsen, P. G. 2008, *A&A*, 486, 437
- Lee, Y.-W., Joo, J.-M., Sohn, Y.-J., Rey, S.-C., Lee, H.-C., & Walker, A. R. 1999, *Nature*, 402, 55
- Lehnert, M. D., Bell, R. A., & Cohen, J. G. 1991, *ApJ*, 367, 514
- Lyons, M. A., Bates, B., Kemp, S. N., & Davies, R. D. 1995, *MNRAS*, 277, 113
- Marino, A. F., Villanova, S., Piotto, G., Milone, A. P., Momany, Y., Bedin, L. R., & Medling, A. M. 2008, *A&A*, 490, 625
- Milone, A. P. et al. 2008, *ApJ*, 673, 241
- Monaco, L., Pancino, E., Ferraro, F. R., & Bellazzini, M. 2004, *MNRAS*, 349, 1278
- Moretti, A. et al. 2008, *A&A*, 493, 539
- Norris, J. E. & Freeman, K. C. 1983, *ApJ*, 266, 130
- Norris, J. E., Freeman, K. C., & Mighell, K. J. 1996, *ApJ*, 462, 241
- Pancino, E., Ferraro, F. R., Bellazzini, M., Piotto, G., & Zoccali, M. 2000, *ApJ*, 534, L83
- Pasquini, L., et al. 2002, *The Messenger*, 110, 1
- Peterson, R. C., & Cudworth, K. M. 1994, *ApJ*, 420, 612
- Pietrinferni, A., Cassisi, S., Salaris, M., & Castelli, F. 2004, *ApJ*, 612, 168
- Pilachowski, C., Wallerstein, G., Leep, E. M. & Peterson, R. C. 1984, *ApJ*, 263, 187
- Piotto, G., Villanova, S., Bedin, L. R., Gratton, R., Cassisi, S., Momany, Y., Recio-Blanco, A., Lucatello, S., Anderson, J., King, I. R., Pietrinferni, A., & Carraro, G. 2005, *ApJ*, 621, 777
- Piotto, G. et al. 2007, *ApJ*, 661, L53
- Piotto, G., 2008, *Mem. Soc. Astron. Ital.*, 79, 334
- Piotto, G. 2009, *arXiv:0902.1422*
- Piotto, G. et al. 2009, in preparation
- Pryor, C., & Meylan, G. 1993, *Structure and Dynamics of Globular Clusters*, 50, 357
- Ramírez, S. V., & Cohen, J. G. 2002, *AJ*, 123, 3277
- Sarajedini, A., et al. 2007, *AJ*, 133, 1658
- Suntzeff, N. B., & Kraft, R. P. 1996, *AJ*, 111, 1913
- Villanova, S. et al. 2007, *ApJ*, 663, 296
- Yong, D., & Grundahal, F. 2008, *ApJ*, 672, L39